Physicochem. Probl. Miner. Process., 59(6), 2023, 174415

http://www.journalssystem.com/ppmp

Physicochemical Problems of Mineral Processing

ISSN 1643-1049
© Wroclaw University of Science and Technology

Adsorption of hydrated $Fe(OH)_2^+$ on the kaolinite surface: A density functional theory study

Hongqiang Wu [1,2], Yuqi Miao [1,4], Qibang Long [1], Huashan Yan [1,3], Yong Li [1], Sen Qiu [1], Hao Wu [1], Guanfei Zhao [1,3], Tingsheng Qiu [1,3]

[1] School of Resource and Environmental Engineering, Jiangxi University of Science and Technology, Ganzhou 341000, China

[2] Sinosteel Maanshan Mining Research Institute Co., Ltd., Maanshan 243000, China

[3] Collaborative Innovation Center for Development and Utilization of Rare Metal Resources Co-sponsored by Ministry of Education and Jiangxi Province, Jiangxi University of Science and Technology, Ganzhou 341000, China

[4] School of Chemical Engineering, Zhengzhou University, Zhengzhou 450001, China

Corresponding authors: jxustyhs@163.com (Huashan Yan), qiutingsheng@163.com (Tingsheng Qiu)

Abstract: The present study employed density functional theory (DFT) to analyze the adsorption configuration and mechanism of $Fe(OH)_2^+$ on the kaolinite (001) surface. The findings demonstrated that $Fe(OH)_2(H_2O)_4^+$ is the main type in which hydrated $Fe(OH)_2^+$ can be found in aqueous solution. On the surface of kaolinite, $Fe(OH)_2(H_2O)_4^+$ will be adsorbed. There are two forms of adsorption: outer-sphere and inner-sphere coordination (monodentate/bidentate) adsorption. $Fe(OH)_2(H_2O)_4^+$ has a moderate propensity to adsorb on the alumina octahedral sheet of kaolinite when the outer-sphere coordination adsorption takes place. In cases of inner-sphere coordination adsorption, Fe exhibits a tendency to form monodentate adsorption compounds in conjunction with O_u atoms. Additionally, it prefers to create bidentate adsorption compounds through coordination with both O_t and O_u atoms. The adsorption mechanism analysis results show that the ionic property of Fe atom decreases after outer-sphere coordination adsorption. After inner-sphere coordination adsorption, some electrons of Fe atom are transferred to the surface O atom. The presence of electrons between the Fe and O atoms enhances the formation of bonds, hence enhancing the covalent nature of the Fe-O bond. Theoretical FT-IR (Fourier transform infrared spectroscopy) calculations show that the formation of Fe-O chemical bonds. Because of the lower adsorption energy and more chemical bonds, hydrate $Fe(OH)_2^+$ is more likely to be bidentate adsorbed on the kaolinite surface.

Keywords: kaolinite, adsorption, Fe, density functional theory

1. Introduction

Rare earths (especially medium and heavy rare earths) are of great strategic significance in the national defense industry and some high-tech fields. Ionic rare earth ores are rich in medium and heavy rare earth elements (Zhang et al., 2021; Luo et al., 2014;), and rare earth ions exist in the form of ion adsorption on clay minerals. Highly reactive cations like Mg^{2+}, NH_4^+, and similar species have the capacity to facilitate the desorption of rare earth ions from the surfaces of clay minerals into the leachate solution. (Wang et al., 2021) But in this process, other metal ions adsorbed on the clay minerals surface (especially Al^{3+}, Fe^{3+}) can be desorption into the leachate in large quantities, which will seriously affect the quality of rare earth products (Qiu et al., 2014). Although researchers have carried out a lot of research on impurity inhibitors and impurity leaching technology, it will still cause the loss of rare earth resources while leaching (Qiu et al., 2014; Fang et al., 2018; Fang et al., 2012; Zhou et al., 2022; Wu et al., 2021; Zhao et al., 2007; Xu et al., 2005; Yin et al., 2012;). To enhance the efficiency of rare earth resource recovery and optimize the use rate of these resources, the occurrence state and adsorption mechanism of impurity metal ions in ionized rare earth minerals need to be studied, so as to further develop rare earth leaching agents with high selectivity.

DOI: 10.37190/ppmp/174415

In recent decades, researchers have conducted extensive research on adsorbent adsorption on the surface of clay minerals. Dousova et al. (2011) investigated the adsorption affinity for As oxyanions after Fe/Al/Mn pretreatment of clay minerals using low-grade calcined kaolin (MT) and bentonite (BT). To transform the surface charge of sodium smectite clays from negative to positive, ferric ions (Argel-Fe and Volclay-Fe) were added. Rodrigues et al. (2020) tested clay in a synthetic wastewater containing seven anionic dyes (a mixture of tartar, brilliant blue FCF, and amaranth). The maximum adsorption capacities for Argel-Fe were 88.68 mg g(-1) and 392.21 mg g(-1) for Volclay-Fe, while enrichment of clays with Fe(III) enhanced functionality to the clays and produced adsorbents with quick adsorption abilities and high discoloration capacities. Neumann et al. (2013) investigated electron transfer from Fe(II) sorbed to basal planes and edge OH-groups of the clay mineral NAu-1 using mossbauer spectroscopy in conjunction with selective chemical extractions. The results demonstrate that Fe(II) sorbed primarily to basal planes at pH values less than 6.0 and to edge OH-groups at pH values more than 7.5. At pH 7.5, significant electron transfer occurred from edge OH-group bound Fe(II), but at pH 4.0 and 6.0, electron transfer from basal plane-sorbed Fe(II) to structural Fe(III) occurred but to a considerably lesser amount than from edge-bound Fe(II). Feng et al. (2023) investigated how Fe co-adsorption affected the mechanism of REE uptake on kaolinite using inductively coupled plasma mass spectrometry (ICP-MS), powder X-ray diffraction (PXRD), and X-ray photoelectron spectroscopy (XPS).The findings indicate that FeOOH layers formed on top of REEs on the surface of kaolinite, and Fe is deleterious to REE ion-exchange efficiency. Experiments were used in the preceding investigations. Quantum chemistry can study compound reaction processes and the structural properties of molecules at the atomic level. It includes ab initio algorithm, semi-empirical method and density functional theory method (Yan et al., 2019;). The density functional theory (DFT) method, which is suitable for the simulation calculation of large molecular systems and solids and has been widely utilized in mining, the chemical industry, and other industries, requires less calculation than the first two quantum chemical methods. It has also been used to study the adsorption configuration and mechanism of various adsorbents on mineral surfaces, such as the adsorption of Y^{3+}、Lu^{3+}、Al^{3+}、Pb^{2+} and $CaOH^{+}$ on kaolinite surface (Qiu et al., 2021; Miao et al., 2022; Fang et al., 2020; Wang et al., 2014; Peng et al., 2017; Zhang et al., 2021; Jiang et al., 2023). The microscopic mechanism of Fe occurrence on the surface of clay minerals is rarely studied. It is critical to investigate the adsorption mechanism of Fe on the clay material surface since it is a typical impurity ion in rare earth leaching solutions. Vitaly et al. (2022) apply density functional theory (DFT) calculations to provide atomistic insights into the heterogeneous reaction between aqueous Fe(II) and the Fe-bearing clay mineral nontronite $Fe_2Si_4O_{10}(OH)_2$ by studying its adsorption mechanism and interfacial Fe(II)−Fe(III) electron transfer (ET) at edge and basal surfaces. Using DFT and molecular-dynamics simulation techniques, Liu et al. (2012) investigated the inner-sphere coordination adsorption of Fe^{2+} on the edge surfaces of kaolinite. However, this study did not consider the hydroxylation of Fe^{2+}, and only the edge surface of kaolinite was studied. Fe, a significant contaminant in the processing of rare earths, can be found on the surface of carrier minerals in a variety of forms, primarily as a hydrated hydroxyl group in solution. The most common mineral for transporting rare earth ions is kaolinite, which is also the mineral that dissociates most readily in the 001 direction. Therefore, it is essential to investigate the hydrated hydroxyl iron's adsorption behavior on the kaolinite (001) surface.

Using a density generalized function theory analysis based on the firstness principle, the adsorption configuration of dihydroxy hydrates of Fe^{3+} on kaolinite (001) surface and its fugacity mechanism on kaolinite surface were explored in this paper (Mulliken et al., 1955). The findings of this research contribute to the understanding of the metallogenic mechanism of ion-type rare earth ore. Additionally, they provide valuable insights for addressing the issue of iron impurities in ion-type rare earth ore. Furthermore, these results can be utilized as a reference for the development of iron inhibitors or more effective leaching agents.

2. Materials and methods

The CASTEP module of Materials Studio 2019 was used to do the calculations, which were based on density functional theory first-principles. The cut-off energy is selected to 400 eV during computation following the convergence test and in accordance with the results (Hohenberg et al., 1964; Kohn et al., 1964; Clark et al., 1964). Ultrasoft pseudopotentials were employed for density generalization

calculations, utilizing the WC generalization method within the framework of the generalized gradient approximation (GGA) (Wu et al., 1964; Ireta et al., 2004; Vanderbilt et al., 1990). The convergence value of the Self-Consistent Field (SCF) was determined to be 2.0×10^{-6} eV·atom^{-1}, and the energy, atomic forces, and atomic displacements were all improved using the BFGS method. Structure optimisation and convergence tolerances for energy calculations were set at 2.0×10^{-5} eV·atom^{-1} for energy convergence, 0.05 eV^{-1} for interatomic force convergence, 0.002 for atomic displacement convergence, and 0.1 GPa for intracrystal stress convergence. (Monkhorst et al., 1990; Pack et al., 1976; Pfrommer et al., 1997; Yin et al., 1997; He et al., 2021). Kaolinite's bulk type and surface's Brillouin zone integrals were estimated to be (2×1×3) and (2×1×1), respectively (Neder et al., 1999; Wu et al., 1964; Ireta et al., 2004). This investigation used the Monkhorst-Pack k-point grid sampling approach, as described by Zhang et al. (2021; 2021). The structure of kaolinite was investigated using neutron powder diffraction at a low temperature of 1.5 K based on experimental data. The obtained structural parameters were: a = 10.40, b = 18.03, c = 25.30, α= 90°, β= 90°, and γ= 89.73°. The computer software applies dipole moment correction within an electrically neutral adsorption system to establish spin polarization (Luo et al., 2022).

Modeling of kaolinite crystals for geometric optimization. Cutting the optimum cell model along the 0 0 1 direction produced the Kaolinite (001) surface, which was then covered with a vacuum layer with a 20 Å height to eliminate interlayer interactions. To accurately describe the ion-surface interactions, a 2×2×1 supercell was created and geometrically optimized. Due to the small depth of ion-surface interaction, the alumina octahedral sheet and silica tetrahedral sheet of kaolinite were fixed separately for the surface optimization in order to save computational cost. After the optimization, the stabilization models of silica tetrahedral sheet and alumina octahedral sheet were obtained respectively, in which three forms of hydroxyl groups appeared on the alumina octahedral sheet. As illustrated in Fig. 1, the three distinct arrangements of hydroxyl groups are labeled as "lying" (O_l), "tilted" (O_t), and "up" (O_u).

In order to make the process of adsorption closer to the real situation, we placed $Fe(OH)_2^+$ in a 15×15×15 Å^3 periodic box and added 1 to 7 water molecules for each calculation. The atomic force, energy, and displacement converging criteria were 0.03 eV/atom, 1.0×10^{-5} eV/atom, and 0.001 Å, respectively. The binding energy (E_{bind}), which is defined as follows (1), is used to assess the stability of the $Fe(OH)_2^+$ hydrate model, represented as $[Fe(OH)_2(H_2O)_n]^+$ ($1 \le n \le 7$).

$$E_{bind} = E_{[Fe(OH)_2(H_2O)_n]^+} - E_{Fe(OH)_2} - nE_{H_2O} \quad (1)$$

where E_{bind} is the binding energy of hydrate $Fe(OH)_2^+$, $E_{[Fe(OH)_2(H_2O)n]^+}$, E_{Fe} and E_{H_2O} correspond to the energy of the entire system, $Fe(OH)_2^+$, and H_2O, respectively.

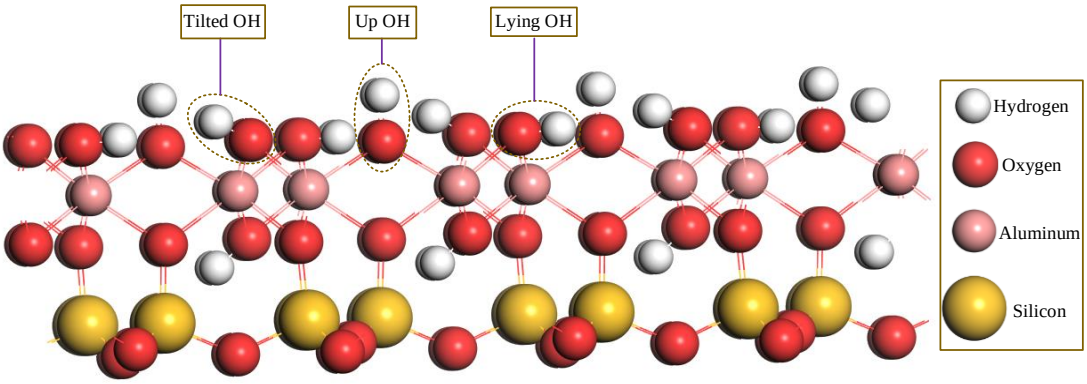

Fig. 1. The optimized surface model of 2×2×1 kaolinite surface

After obtaining a stable model of hydrated $Fe(OH)_2^+$, the method of adsorption of the dependable structure of $Fe(OH)_2^+$ on the alumina octahedral and silica tetrahedral sheets was examined. Two types of adsorption models were study: outer-sphere and inner-sphere coordination adsorption. When computing the outer-sphere coordination adsorption on the alumina octahedral sheet, hydrated $Fe(OH)_2^+$ is placed precisely above the center of the three hydroxyl groups on the surface. When computing the outer-sphere coordination adsorption on the silica tetrahedral sheet, the hydrated $Fe(OH)_2^+$ were placed precisely above the core of the six-membered silicon-oxygen ring. Adsorption

compounds that are formed are referred to as "M" and "N", respectively. When calculating the monodentate adsorption of the adsorbate, a water in the adsorbate is removed, the adsorbate was placed directly above the three deprotonated hydroxyl oxygen atoms. When calculating the bidentate adsorption of the adsorbate on the alumina octahedral sheet, two water ligands in the adsorbate is removed, the adsorbate was placed above the bridge position between the two deprotonated hydroxyl groups, respectively. Fig 2 shows the initial inner-sphere coordination adsorption position. As can be seen from the figure, $Fe(OH)_2^+$ may undergo monodentate adsorption on three different hydroxyl groups to form monodentate adsorption compounds and may undergo bidentate adsorption on the bridge sites between two adjacent hydroxyl groups to form bidentate adsorption compounds. The compounds formed at the "O_l", "O_u" and "O_t" sites are named L, U and T. The compounds formed at the "O_u-O_t", "O_u-O_l" and "O_t-O_l" sites are named as UT, UL and TL. The adsorption energy (E_{ads}) is used to characterize whether adsorption can occur on the surface and the strength of adsorption. A positive value of adsorption energy means that adsorption cannot occur. A negative value of adsorption energy means that adsorption can take place, and the more negative the value, the more likely adsorption will take place. E_{ads} can be can be calculated by formula (2) (He et al., 2023; Qiu et al., 2021; Miao et al., 2022;).

$$E_{ads} = E_{Fe/S} - E_{Fe} - E_S \quad (2)$$

where E_{ads} is the adsorption energy, $E_{Fe/S}$ stand for the total energy of adsorption system, E_{Fe} stand for the total energy in an isolated system of hydrated $Fe(OH)_2^+$. E_S stand for the isolated single-layer kaolinite (001) surface total energy.

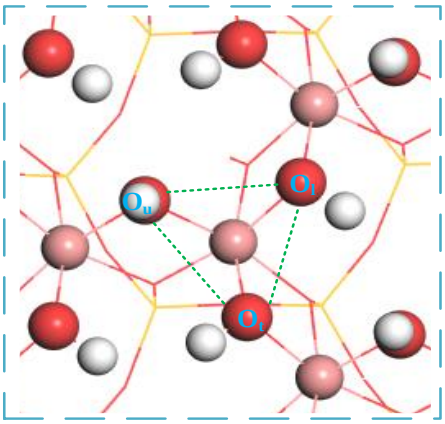

Fig. 2. Initial adsorption position of inner-sphere coordination adsorption

3. Results and discussion

3.1. The form of $Fe(OH)_2^+$ in water environment

Relevant studies have shown that metal ions are difficult to exist in the form of single ion in aqueous solution, and in most cases exist in the form of hydration or hydroxyl hydration. Fig. 3 shows the geometric configuration of $Fe(OH)_2^+$ present in aqueous solution, represented by $Fe(OH)_2(H_2O)_n^+$ (n = 0–7). As illustrated in Fig. 3, coordination links between Fe atoms and O atoms in the surrounding water molecules develop in the first solvated shell layer of $Fe(OH)_2^+$. As the number of water molecules grows from 1 to 4, these bonds become more evenly distributed around $Fe(OH)_2^+$. When there are four water molecules present, a molecule with a shape like an octahedron is created. In instances when the quantity of water molecules exceeded four, it was discovered that the coordinated water molecules were situated at a considerable distance from the initial solvated shell layer of $Fe(OH)_2^+$. Consequently, $Fe(OH)_2^+$ exhibited coordination with a maximum of four water molecules within the first solvated shell layer of $Fe(OH)_2^+$.

Table 1 presents the equilibrium geometry parameters and binding energies (E_{bind}) associated with several hydrated $Fe(OH)_2^+$ species. According to the data presented in Table 1, there is a clear trend observed as the number of water molecules surrounding $Fe(OH)_2^+$ grows from 1 to 4. Specifically, the maximum distance, minimum distance, and average distance between Fe and O (O_w) in water molecules, as well as the charge of Fe, exhibit a progressive increase. Conversely, the binding energy

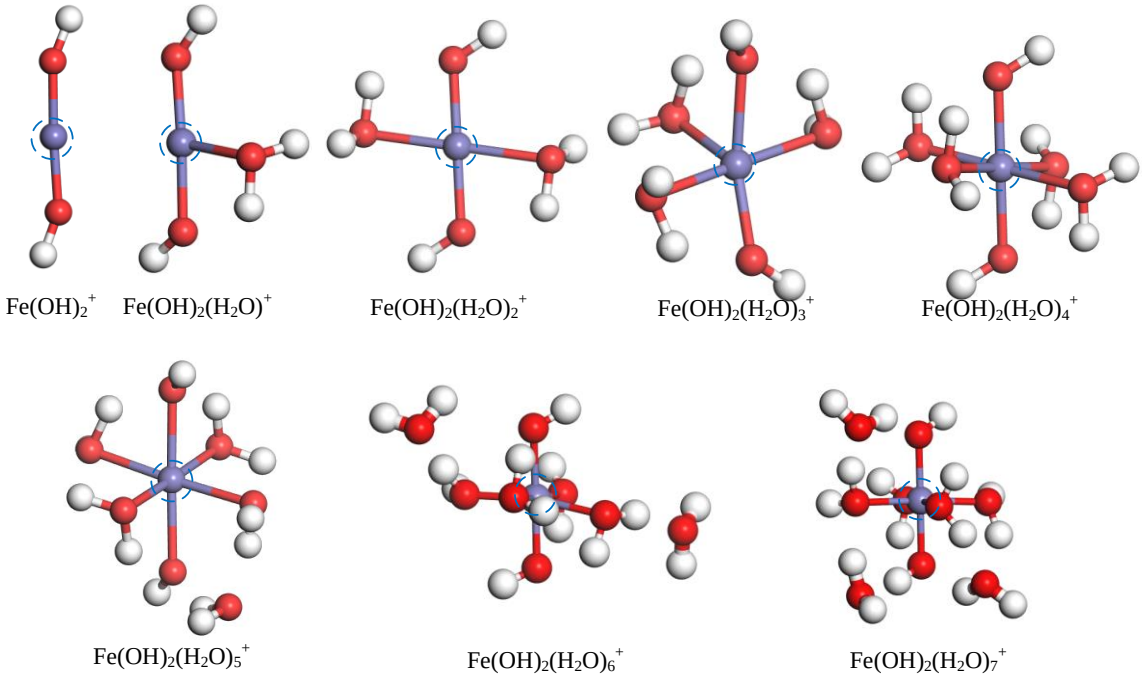

Fig. 3. Geometric configuration of $Fe(OH)_2(H_2O)_n^+$ (n = 0–7)

(E_{bind}) consistently decreases across this range. When the coordination number of water molecules surrounding $Fe(OH)_2^+$ grows to five, there is a significant increase in the maximum distance between Fe and O_w, from 1.969 Å to 3.467 Å. Additionally, the average distance between Fe and O_w also increases, from 1.969 Å to 2.272 Å. The phenomenon of E_{bind} experiences a notable upward trend. The steric-hindrance effect between water molecules and between water molecules and hydroxyl groups is minimal when there are few water molecules surrounding $Fe(OH)_2^+$. The quantity of water molecules increased, and the steric-hindrance effect increased. The water molecules crowd each other in order to stabilize their presence around $Fe(OH)_2^+$ resulting in a gradual increase in the distance between Fe and O_w. As the number of water molecules increases to 4, the E_{bind} continuously decreases from -702.39 to -1042.54 KJ/mol. The E_{bind} is smallest when Fe is coordinated with 4 water molecules, implying that the $Fe(OH)_2(H_2O)_4^+$ formed at this time is the most stable. When the number of water molecules in a system rises over four, a phenomenon known as steric hindrance becomes more pronounced. This results in the inability of water molecules to occupy the initial solvated shell layer of the $Fe(OH)_2^+$. As a consequence of this, they migrate away from the range of bonding that can occur between the atoms of iron and oxygen, which results in an increase in the maximum bond length of iron increased. At this

Table 1. Equilibrium geometry parameters and binding energy values for $Fe(OH)_2(H_2O)_n^+$ species, where n ranges from 1 to 7

n	$R(Fe\text{-}O_w)_{min}$[a]/Å	$R(Fe\text{-}O_w)_{max}$[b]/Å	$R(Fe\text{-}O_w)_{mean}$[c]/Å	Q_{Fe}[d]	E_{bind}/KJ·mol
1	1.886	1.886	1.886	1.20	-702.39
2	1.875	1.930	1.903	1.23	-865.99
3	1.944	1.969	1.954	1.26	-1036.33
4	1.968	1.969	1.969	1.38	-1042.54
5	1.917	3.467	2.272	1.39	-717.17
6	1.826	4.026	3.212	1.37	-806.60
7	1.842	3.391	2.058	1.36	-463.10

[a] The minimum separation distance observed

[b] The maximum separation distance observed

[c] The average distance observed

[d] The charge of Fe

time, the E_{bind} suddenly jumps up to -717.17 KJ/mol, which indicates that the coordination of $Fe(OH)_2^+$ with five water molecules is not in the user's advantage. In conclusion, it can be inferred that the $Fe(OH)_2^+$ species attains its highest stability in an aqueous environment when coordinated with four water molecules, resulting in the production of $Fe(OH)_2(H_2O)_4^+$. Therefore, $Fe(OH)_2(H_2O)_4^+$ was selected as the initial adsorbent for investigating the adsorption behaviour of $Fe(OH)_2^+$ on the surface of kaolinite in the conducted study.

3.2. Outer-sphere coordination adsorption

The kaolinite (001) surface comprises two distinct layer, silica tetrahedral sheet and alumina octahedral sheet, and the adsorbent can be outer layer adsorbed on both surfaces. Consequently, a comprehensive investigation was conducted to examine the adsorption configurations and processes of $Fe(OH)_2(H_2O)_4^+$ on both the silica tetrahedral and alumina octahedral sheets of kaolinite individually. The findings of the investigation are depicted in Fig. 4 and Table 2. As depicted in picture 4, the adsorbent's approach to the surface results in the formation of hydrogen bonds between the oxygen (O) and hydrogen (H) atoms of the adsorbent and the hydrogen (H) and oxygen (O) atoms of the kaolinite surface. This bonding interaction occurs within the specified range, as indicated by the black dashed line in the image. There are two types of hydrogen bonds, the O_s-H_w type hydrogen bond formed between the surface O (O_s) and the H (H_w) atoms of the adsorbent, and the O_w-H_s type hydrogen bond formed between the O (O_w) atoms of the adsorbent and the surface H (H_s). Related studies have shown that interatomic interactions occur in the range of 3 Å. In order to investigate the length and number of hydrogen bonds formed, the maximum bonding length (2.58 Å), which is the default of the software, was used to investigate the hydrogen bonding state generated during the outer-sphere coordination adsorption. The results obtained from the calculations are presented in Table 2. It is evident from the table that the adsorption of the adsorbent onto the Silica tetrahedral sheet resulted in the formation of O_s-H_w type hydrogen bonds with lengths of 1.917 and 2.451 Å. The adsorption of the adsorbent on the alumina octahedral sheet resulted in the formation of hydrogen bonds of O_s-H_w type with lengths ranging from 1.613 to 2.412 Å, and O_w-H_s type with lengths ranging from 1.462 to 2.334 Å. The adsorption of the adsorbent on the alumina octahedral sheet resulted in the formation of hydrogen bonds that were both shorter in length and more abundant as compared to the adsorption on the silica tetrahedral sheet. The increased occurrence of hydroxyl groups in the alumina octahedral sheet contributes to a higher likelihood of interaction between the hydrogen and oxygen atoms in these groups and the oxygen and hydrogen atoms in the adsorbent. Consequently, a greater number of hydrogen bonds are formed.

Following the process of adsorption, it was seen that $Fe(OH)_2^+$ retained coordination with four water molecules. The mean separation distance between iron (Fe) atoms and oxygen (O_w) atoms exhibited variations within the range of 0.003–0.029 Å. The adsorption energy of adsorbate on the silica tetrahedral and alumina octahedral sheet was determined to be -580.50 and -590.53 KJ/mol, respectively. The adsorption energy of the adsorbent on the alumina octahedral sheet exhibits a marginal decrease compared to that on the silica tetrahedral sheet, with a difference of around 1.73%.

In a general sense, it can be observed that the adsorbent formed a greater quantity of hydrogen bonds with shorter bond lengths on the alumina octahedral sheet in comparison to the adsorption of adsorbate on the silica tetrahedral sheet. Additionally, the adsorbent exhibited a lower adsorption energy on the alumina octahedral sheet as opposed to the silica tetrahedral sheet. Hence, the adsorption of adsorbate on the kaolinite (001) surface primarily occurs by outer-sphere coordination, with a minor inclination towards adsorption in the alumina octahedral sheet.

The investigation focused on analysing the partial density of states of Fe, silica tetrahedral sheet, and alumina octahedral sheet in order to get insights into the adsorption mechanism. Fig. 5 (A) displays the density of states for both iron (Fe) and the silica tetrahedral sheet. Following the process of adsorption, it was seen that the 3d orbital of iron (Fe) underwent a little displacement towards higher energy levels. Additionally, the locality of the 3d orbital experienced a modest increase. Simultaneously, it can be shown that the 3d orbital of iron (Fe) retains a significant contribution at the Fermi level, suggesting that Fe maintains a substantial amount of reactivity even after being adsorbed onto the silica tetrahedral sheet. Following the process of adsorption, it was seen that the overall density functional theory (DFT) of the silica tetrahedral sheet saw a downward shift in energy. Additionally, there was a modest rise in

the non-locality of the 2s and 2p orbitals. These findings suggest that the silica tetrahedral sheet achieved a higher level of stability.

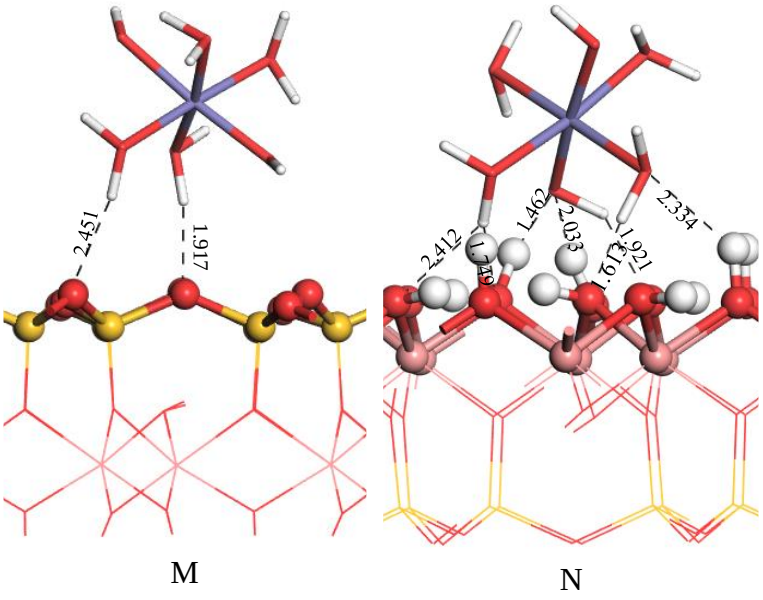

Fig. 4. Outer-sphere coordination adsorption conformation on silica tetrahedral (M) and alumina octahedral sheet (N), respectively

Table 2. Target structural parameters (Å) and adsorption energy (KJ/mol) of hydrated $Fe(OH)_2^+$ outer-sphere coordination adsorption on silica tetrahedral (M) and alumina octahedral sheet (N)

Form	M[a]	$(Fe\text{-}O_w)_{mean}$[b]/Å	$O_s\text{-}H_w$/Å	$O_w\text{-}H_s$/Å	E_{ads}/KJ·mol
M	4	1.966	1.917,2.451	/	-580.50
N	4	1.998	1.613,1.921 1.749,2.412	1.462, 2.033,2.334	-590.53

[a] The quantity of water molecules around Fe

[b] The average distance between the Fe and O atoms in the water ligand

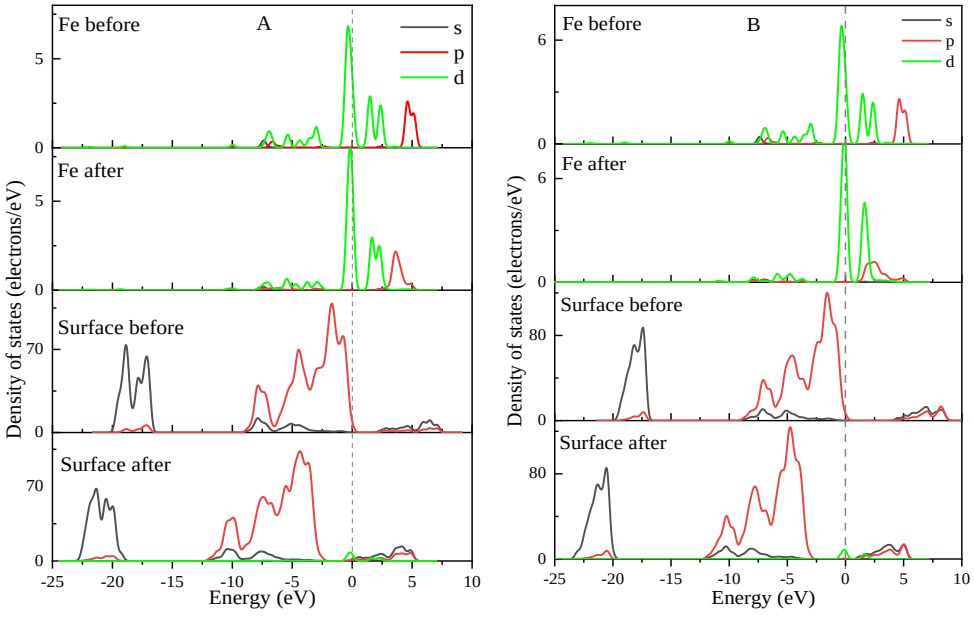

Fig. 5. The PDOS of outer-sphere coordination adsorption of Fe with silica tetrahedral sheet (A) and alumina octahedral sheet (B)

Fig. 5 (B) illustrates the density of states on the Fe and alumina octahedral sheet. The activity of Fe atoms remains very high following their adsorption onto the alumina octahedral sheet, a characteristic that is comparable to their adsorption onto the silica tetrahedral sheet. The DFT of the alumina octahedral sheet clearly changes to the lower energy direction, with a larger amplitude than that of the silica tetrahedral sheet. The findings indicate that iron (Fe) exhibits a minor propensity to adsorb onto the alumina octahedral sheet, resulting in the formation of a more stable outer-sphere coordination adsorption compound.

Table 3 presents the Mulliken charge population analysis of the outer-sphere coordination adsorption on two distinct surfaces. According to the data presented in Table 3, it is evident that the Fe 3p orbital experienced a loss of 0.02 electrons, while the Fe 3d orbital gained 0.1 electrons following the outer-sphere coordination adsorption of adsorbate on the silica tetrahedral sheet. Additionally, Fe exhibited an overall gain of 0.08 electrons after adsorption, resulting in a decrease in its charge by 0.08 and a decrease in ionicity. On the other hand, when hydrated $Fe(OH)_2^+$ was adsorbed on the alumina octahedral sheet, the Fe 3s orbital gained 0.01 electrons, the Fe 3d orbital gained 0.28 electrons, and the Fe 3p orbital lost 0.03 electrons. Consequently, Fe displayed an overall gain of 0.26 electrons after adsorption, leading to a decrease in its charge by 0.26. In comparison to adsorption on the silica tetrahedral sheet, Fe received more electrons, and its ionicity is lower and more stable.

Table 3. Mulliken charge population of Fe atom after outer-sphere coordination adsorption

Site	State	s	p	d	Total	Charge/e
Silica layer	Fe before	0.21	-0.07	6.49	6.63	1.37
	Fe after	0.21	-0.09	6.59	6.71	1.29
	Change	0.00	-0.02	0.10	0.08	-0.08
Alumina layer	Fe before	0.21	-0.07	6.49	6.63	1.37
	Fe after	0.22	-0.10	6.77	6.89	1.11
	Change	0.01	-0.03	0.28	0.26	-0.26

3.3. Inner-sphere coordination adsorption

3.3.1. Monodentate adsorption structure

Since all three different hydroxyl groups on the alumina octahedral sheet of kaolinite (001) can be deprotonated, the deprotonated kaolinite surface can be coordinated with iron ions, thus allowing the inner-sphere coordination adsorption of iron ions on the alumina octahedral sheet of kaolinite. The absorbent has the capability to undergo monodentate adsorption on the "O_l", "O_u", and "O_t" sites of the kaolinite surface, resulting in the formation of three distinct monodentate adsorption compounds. The investigation focused on the monodentate adsorption configuration of the adsorbate on the alumina octahedral sheet of kaolinite. The findings of this investigation are presented in Fig. 6.

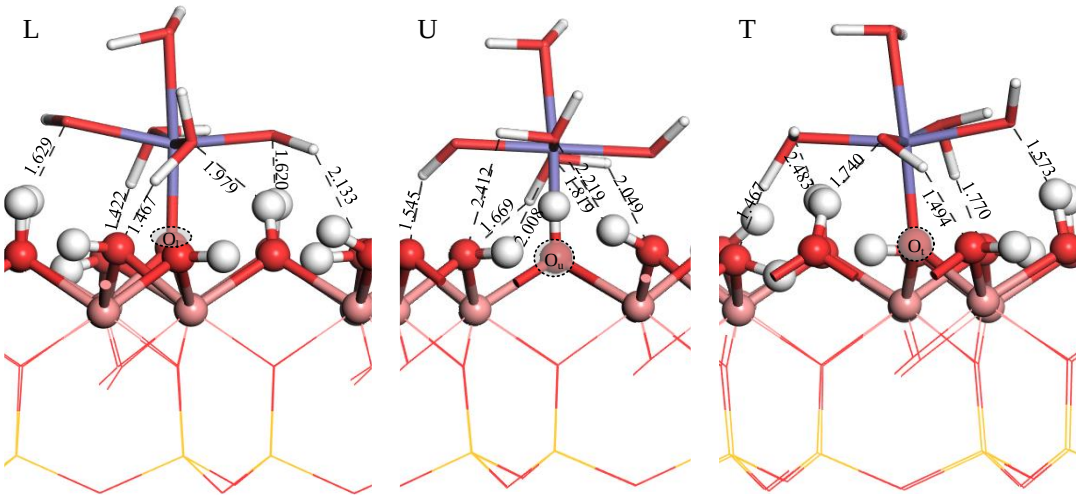

Fig. 6. Monodentate adsorption configuration of absorbent at "O_l" (L), "O_u" (U) and "O_t" (T) positions

As shown in Fig. 6, Fe atoms form coordination bonds with surface deprotonated O atoms after adsorption. Compared to the outer-sphere coordination adsorption process, hydrogen bonds were formed between O_w and H_w atoms in the adsorbent and hydroxyl groups on the kaolinite surface in the default bonding range of the system (0–2.58 Å) (black dashed lines in Fig. 6) during the inner-sphere coordination adsorption process. Table 4 displays the structural parameters and adsorption energies of the adsorption compounds formed. The table reveals that the length ranges of the "O_s...H_w" bonds are 1.422–2.133 Å, 1.467–1.770 Å, and 1.545–2.412 Å, respectively, while the length ranges of the "O_w...H_s" bonds are 1.620–1.979 Å, 1.573–2.483 Å, and 1.819–2.219 Å, respectively. These observations are made when Fe is adsorbed on "O_l", "O_u", and "O_t". When hydrated $Fe(OH)_2^+$ is adsorbed on "O_u", the length of hydrogen bonds is marginally diminished.

In conjunction with hydrogen bonding, the Fe atom established chemical connections with the O atom located on the kaolinite surface. Chemical bonding exerts a significantly greater influence compared to hydrogen bonding, rendering it of more significance in ensuring the stability of the adsorption compound. According to the data presented in Table 4, the measured bond lengths of Fe-O in the L-, U-, and T-type compounds are 1.879, 1.887, and 2.076 Å, respectively. The Fe-O_s bond length in L and U type compounds has a shorter distance compared to that in C-type compounds, whereas the disparity in chemical bonding between the L- and U-type compounds is relatively smaller. The adsorption energies of compounds L-, U-, and T-type are recorded as -848.27, -861.91, and -855.60 KJ/mol, respectively. In contrast to type L and T compounds, the U type chemical exhibits the most minimal absorption energy.

In general, it is widely accepted that the adsorption of Fe at the "O_u" position leads to the formation of shorter hydrogen bonds, slightly shorter chemical bonds, and lower adsorption energy. Consequently, it is hypothesised that hydrated $Fe(OH)_2^+$ is more prone to adsorb onto the "O_u" position, resulting in the formation of a U-type adsorption compound during monodentate adsorption on the surface of kaolinite.

Table 4. Structure parameters (Å) and adsorption energy (KJ/mol) of the adsorption compounds

Form	M[a]	Fe-O_s[b]/Å	Fe-O_{oh}[c]/Å	Fe-O_w[d]/Å	O_s-H_w/Å	O_w-H_s/Å	E_{ads}/KJ·mol^{-1}
L	3	1.879	1.855 1.963	1.962,1.964 2.041	1.422,1.467 2.133	1.620,1.629 1.979	-848.27
U	3	1.887	1.840 1.927	2.020,2.041 2.095	1.467,1.494 1.770	1.573,1.740 2.483	-861.91
T	3	2.076	1.835 1.835	1.961,1.964 1.964	1.545,1.669 2.049,2.412	1.819,2.008 2.219	-855.60
UT	1	1.761 1.872	1.759 1.761	2.174	1.650	/	-1537.91
UL	0	1.766 1.771	1.779 1.789	/	1.849	1.870	-1503.97
TL	1	1.710 1.920	1.827 1.864	2.075	/	1.879,2.207	-1507.19

[a] Number of aqua ligands

[b] The measurement of the distance between the iron (Fe) and oxygen (O) on the surface

[c] The length of the bond between Fe and O in a hydroxyl group

[d] The measurement of the distance between Fe and O of aqua ligand

3.3.2. Bidentate adsorption

In the process of bidentate adsorption, iron (Fe) has the capability to create three distinct bidentate adsorption compounds at the "O_u-O_t," "O_u-O_l," and "O_t-O_l" sites, as visually depicted in Fig. 7. In compounds of UT-, UL-, and TL-types, the detachment of water molecules from the initial solvation shell is observed due to the steric hindrance effect. Specifically, one water molecule is detached in UT-type, two water molecules in UL-type, and one water molecule in TL-type compounds. Analogous to monodentate adsorption, the interaction between the adsorbate and the kaolinite surface involves the

formation of hydrogen bonds. The hydrogen bond is illustrated by the black dashed line in Figure 7. The maximum length of a hydrogen bond is set to 2.58 Å. The compounds of types UT and UL have "O_s...H_w" bond lengths measuring 1.650 Å and 1.849 Å, respectively. However, the compound of TL-type does not possess a "O_s...H_w" bond. In the UL-type compound, the bond length between "O_s" and "H_w" is comparatively shorter. The TL-type compound exhibits the formation of two hydrogen bonds, with bond lengths of 1.879 Å and 2.207 Å. On the other hand, the UL-type compound forms a hydrogen bond denoted as "O_w...H_s" which has a bond length of 1.870 Å. The generation of the "O_w...H_s" phenomenon does not occur in the UL-type compound. The "O_w... H_s" present in the TL-type compound exhibit a little greater length, albeit with a higher quantity.

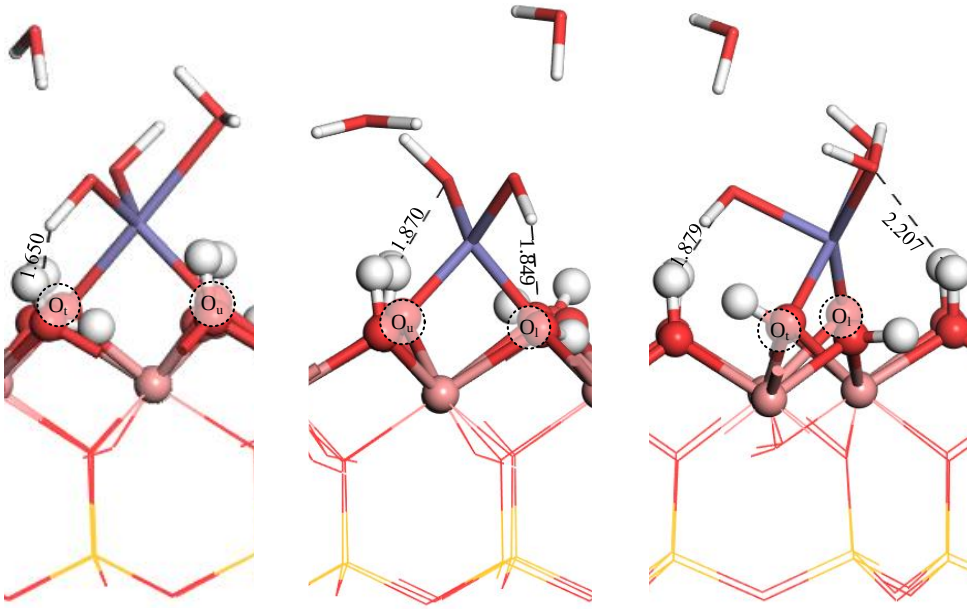

Fig. 7. Bidentate adsorption configuration of absorbent at positions "O_u-O_t" (UT), "O_u-O_l" (UL) and "O_t-O_l" (TL), respectively

The length of "Fe-O_s" in UT-, UL- and TL-types compounds is between 1.761 and 1.872 Å, 1.766 and 1.771 Å, and 1.710 and 1.920 Å, respectively. The chemical bonds formed in the bidentate adsorption compounds are shorter in length and more numerous than those in the monodentate adsorption compounds. Therefore, the bidentate adsorption compounds are more stable from the view of chemical bonding. Among the three types of compounds formed, the chemical bond formed in UL-type compound is slightly shorter.

According to the data presented in Table 4, it can be observed that the adsorption energy associated with bidentate adsorption is significantly lower compared to that of monodentate adsorption. This discrepancy suggests that the bidentate adsorption compound exhibits more stability, implying a higher likelihood for the hydrated Fe species to undergo bidentate adsorption on the surface of kaolinite. The adsorption energy of UT-type compounds exhibits a little decrease in comparison to the other two compounds.

Typically, when the adsorbate is adsorbed at the "O_u-O_t" position, it is observed that the hydrogen bond exhibits a reduced length, the chemical bond experiences a little reduction in length, and the adsorption energy is diminished. Hence, upon comparing the adsorption characteristics of the adsorbate at three distinct locations on the kaolinite (001) surface, it becomes evident that there is a minor inclination for the adsorbate to adsorb at the "O_u-O_t" position.

3.3.3. Adsorption of water molecules on kaolinite surface

Kaolinite has a hydrophilic surface, making it easy to adsorb water molecules and form a hydration film. The adsorption of metal ions on the surface of kaolinite requires displacing the water molecules on the surface before forming an adsorption structure. Therefore, it is necessary to calculate the

adsorption capacity of water molecules on the kaolinite (001) surface (He et al., 2021). By replacing the hydrated $Fe(OH)_2^+$ in the aforementioned adsorption model with water molecules, the adsorption structure and adsorption energy of water molecules on the ideal kaolinite surface and the deprotonated kaolinite surface can be calculated. Finally, it can be determined whether the hydrated $Fe(OH)_2^+$ can replace water molecules on the kaolinite surface.

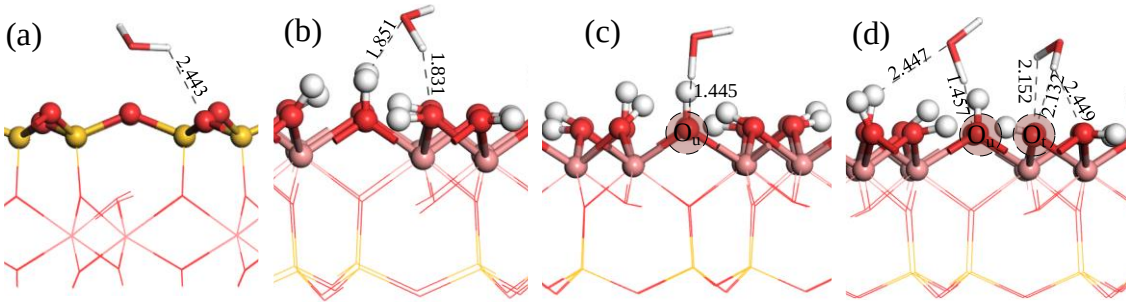

Fig. 8. Adsorption structure of water molecules on kaolinite surface (a: Ideal kaolinite Si-O surface; b: Ideal kaolinite Al-OH surface; c,d: Kaolinite surface with one and two protons removed, respectively)

Table 5. Structure parameters (Å) and adsorption energy (KJ/mol) of H_2O adsorbed on the kaolinite (001) surface

Name	O_s-H_w/Å	O_w-H_s/Å	E_{ads}/ KJ·mol^{-1}
a	2.443	/	-1.82
b	1.831	1.851	-24.87
c	2.140	/	-61.21
d	1.457,2.132 2.152,2.449	2.447	-128.34

From Fig. 8 and Table 5, it can be seen that when water molecules adsorb on the surface of ideal kaolinite, the main interaction occurs through hydrogen bonds formed between the H_w and O_w atoms of water molecules and the O_s and H_s atoms on the kaolinite surface. When water molecules adsorb on the Al-OH surface of ideal kaolinite, they form a O_s-H_w bond with a length of 1.831 Å and O_w-H_s bond with a length of 1.851 Å. On the Si-O surface, water molecules form a O_s-H_w bond with a length of 2.443 Å. The number of hydrogen bonds formed on the Al-OH surface is greater and the strength is stronger. Furthermore, the adsorption energy of water molecules on the Al-OH surface (-24.87 KJ/mol) is much lower than that on the Si-O surface (-1.82 KJ/mol). Both the adsorption structure and adsorption energy results indicate that water molecules are more prone to adsorb on the Al-OH surface of ideal kaolinite. This result is the same as that of chen et al.

When water molecules adsorb on kaolinite surface with one proton removed, they produce an O_s-H_w hydrogen bond with a length of 2.140 Å and an adsorption energy of -61.21 KJ/mol. When water molecules adsorb on kaolinite surface with two protons removed, they produce five O_s-H_w hydrogen bonds with a length ranging from 1.457 to 2.449 Å, and the adsorption energy of a single water particle is -64.17 KJ/mol. The results showed that the higher the degree of deprotonation, the more easily the adsorption of water molecules occurred. However, the adsorption energy of hydrated $Fe(OH)_2^+$ on ideal kaolinite (001) surface (-590.53 KJ/mol) is much lower than that of water molecules on the ideal kaolinite surface (-24.87 KJ/mol). Similarly, the adsorption energy of hydrated $Fe(OH)_2^+$ on the deprotonated kaolinite surface is also much lower than that of water molecules on the deprotonated kaolinite surface. The results show that the hydrated $Fe(OH)_2^+$ can push out the water molecules on the surface of kaolinite, and then adsorb on the surface of kaolinite.

3.3.4. Bonding mechanism

From 3.3.1 and 3.3.2, U-type compound and the UT-type compound are the optimal adsorption structures of the two adsorption modes respectively. These two compounds were chosen to analyze their bonding mechanisms. Table 6 shows the Mulliken populations of Fe and O_s atoms and Mulliken

overlap populations of Fe-O_s bonds in the two predominance adsorption compounds. It can be seen that in the U-type compound, the electronic orbitals (3s and 3d) of the Fe atom lost 0.28 e after adsorption, and the 2p orbitals gains 0.07 e, so the Fe atom as a whole behaves as an electron-deficient state. For the O atom, the 2s orbitals lost 0.05 e, but the 2p orbitals gain 0.20 e, so the O atom as a whole behaves as electron-rich state. Part of the electrons of the Fe atoms are transferred to the O_s atoms, which leads to the enhancement of the ionicity of Fe；

According to the data presented in Table 6, it can be observed that in the UT-type compound, the Fe atom experiences a loss of 0.26 e in both its 3s and 3d orbitals, while its 3p orbital gains 0.07 e. The adsorption process resulted in a total loss of 0.38 electrons by the iron (Fe) atom. O_t lost 0.03 and 0.04 e in its 2s and 2p orbitals, respectively. The overall loss incurred by O_t amounted to 0.07 e. The 2p receives 0.10 e, while the 2s of O_u loses 0.04 e. O_u has a total gain of 0.06 e. Table 7 illustrates the charge transfer mechanisms involving oxygen (O) and hydrogen (H) atoms occurring at the kaolinite surface and within hydrated $Fe(OH)_2^+$. As can be seen in table 7, the O atom in the adsorbate loses a lot of electrons after adsorption, the H atom only gets a small amount of electrons, and the kaolinite surface gets a lot of electrons after adsorption. In general, most of the electrons of O and Fe in the adsorbate are transferred to the kaolinite surface, and the ionicity of Fe is enhanced.

The larger the Mulliken overlap layout value, the more electron overlap between the two atoms, indicating that the chemical bonds formed between the atoms are more stable. The Mulliken overlap layout value in the U-type compound is 0.32, and the values in the UT-type compound are 0.24 and 0.36. the overlap layout value of Fe-O_s in UT-type compound is significantly larger than that of Fe-O_s in U-type compound, indicating that in the bidentate adsorption compound, Fe interacts more strongly with the surface and the formed compound page is more stable, which is the same as the results of the previous study. In addition, since the overlap layout value is all positive, this indicates that the electrons of both Fe and surface O interact in a bonding state, forming covalent bonds.

Table 6. Mulliken populations of Fe and O_s atom and Mulliken overlap populations of Fe-O_s bonds in U-, and UT-type compound

Type	States	Fe					O_t				O_u				Fe-O_s
		s	p	d	Total	Charge/e	s	p	Total	Charge/e	s	p	Total	Charge/e	
U	Before	0.33	-0.02	6.72	7.02	0.98	\	\	\	\	1.91	4.90	6.81	-0.81	0.32
	After	0.23	0.05	6.54	6.82	1.18	\	\	\	\	1.86	5.10	6.97	-0.97	
	Charge	-0.10	0.07	-0.18	-0.20	0.20	\	\	\	\	-0.05	0.20	0.16	-0.16	
UT	Before	0.49	0.00	6.67	7.17	0.83	1.90	4.98	6.88	-0.88	1.91	4.95	6.86	-0.86	0.45
	After	0.23	0.14	6.41	6.79	1.21	1.87	4.94	6.81	-0.81	1.87	5.05	6.92	-0.92	0.32
	Charge	-0.26	0.14	-0.26	-0.38	0.38	-0.03	-0.04	-0.07	0.07	-0.04	0.10	0.06	-0.06	

Table 7. UT-type compound charge transfers (e) of O and H atoms of hydrated $Fe(OH)_2^+$ and kaolinite surface

Form	Qo	Q_H	Qo′	Q_H′	ΔQo^a	ΔQ_H	Q_k	Q_k′	ΔQ_k
UT	-2.72	1.84	-2.42	1.77	0.3	-0.07	-0.08	-0.46	-0.38

[a] Q = Q′-Q, where Q and Q′ are the total charges of H, O and kaolinite surface before and after adsorption, respectively

Fig. 9 (a) and (b) show the differential charge density diagrams between Fe and surface O atoms in the monodentate and bidentate adsorption compound, respectively. The blue part represents electron deficiency and the red part represents electron accumulation. It can be seen from the figure that Fe atoms in the two adsorption compounds are in electron deficiency state, and surface O atoms are in electron accumulation state, indicating that the charge of Fe atoms shifts to the surface O atoms after adsorption. In addition, the red part of O atom appear to shift towards the Fe atom, and the shift pattern of the O atom electrons in (b) is more significant. It is shown that Fe and O atom have strong covalency, and the Fe-O bond formed by bidentate adsorption is stronger than that formed by monodentate adsorption, which is consistent with the Mulliken layout results in Table 6. The study further explored the density of states (PDOS) of Fe and O atoms to confirm the distribution and contribution of electronic states between bonded atoms.

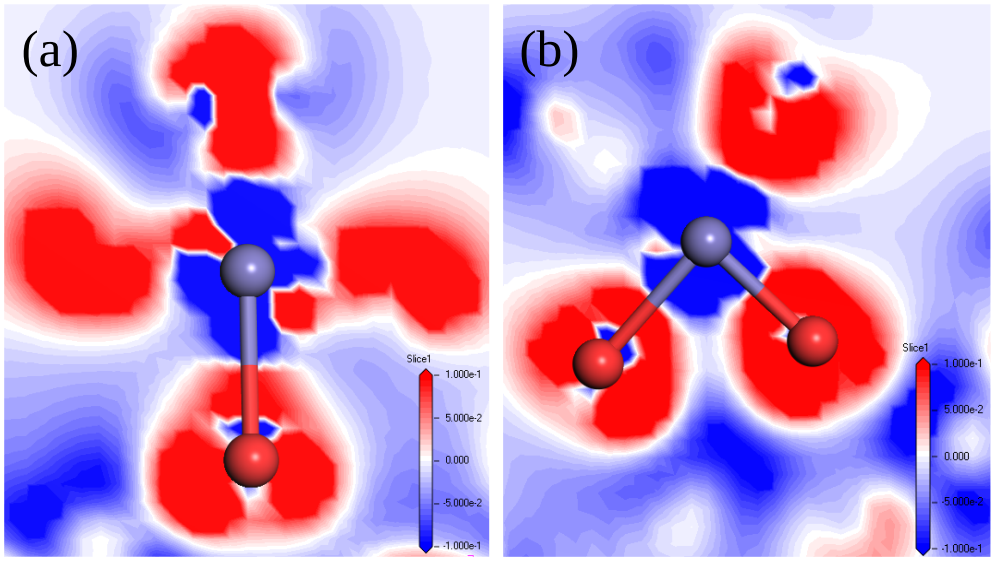

Fig. 9. Differential charge density diagram of U-type (a) and UT-type compounds

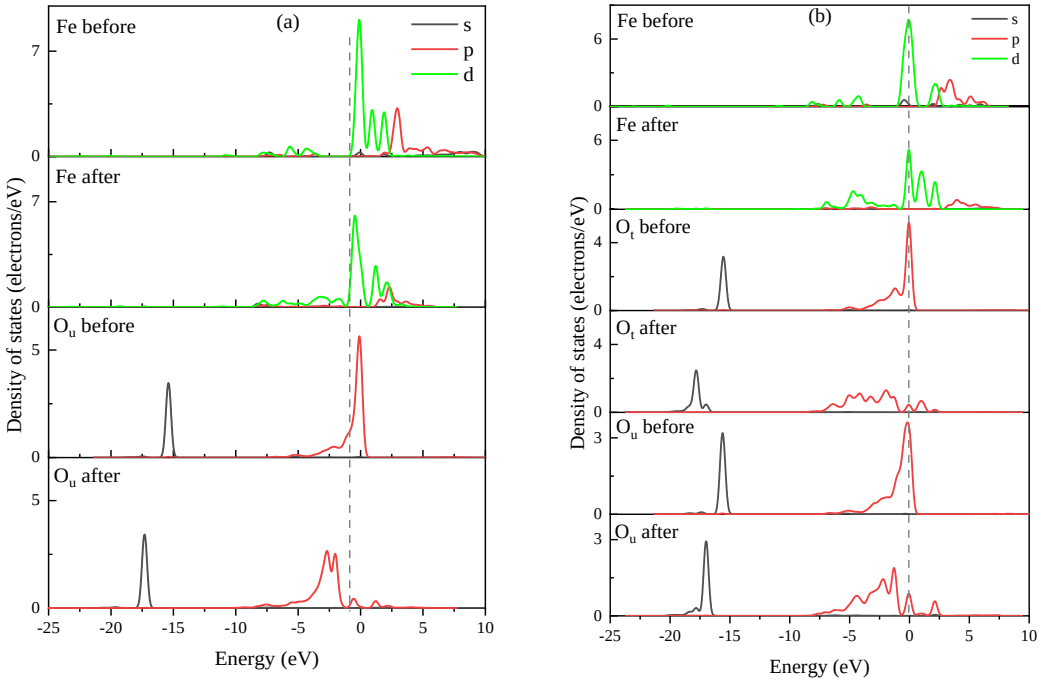

Fig. 10. PDOS of Fe and O atoms in form U (a) and UT (b). The Fermi level is signified by a black dashed line

The non-localization of the Fe 3d orbit and the 2p orbit of the surface O increases noticeably after the monodentate adsorption, as can be observed in Fig. 10(a), meaning that the Fe and the surface O atoms develop less unstable after adsorption. Furthermore, both the density of state of the Fe atom and the O atom of the kaolinite surface shift to the lower energy level. The Fermi level contribution from Fe 3d and 3s orbitals is drastically reduced, indicating that Fe is more secure and the activity is lower. The contribution of the O atom's 2p orbital to the Fermi level is likewise greatly lowered, suggesting that the atom's activity has been significantly reduced as a result of adsorption as well as that it has become more stable. Following adsorption, the O atom yields four consecutive 2p orbital peaks in the -2.5 to 2.5 eV range, a fresh 3d orbital peak in the range of -2.5 to -1.25 eV, and a weak 3d orbital peak in the range of 2.5–2.75 eV. The Fe and surface O atoms form bonding orbitals, shown by the strength of the O 2p orbital peak being stronger than that of the Fe 3d orbital peak in the range of -2.5 to -1.25 eV; a weak 3d orbital peak appears at 2.5–2.75 eV; and the O atom yields four consecutive 2p orbital peaks in the range of -2.5 to 2.5 eV. O 2p orbital peak strength is higher than Fe 3d orbital peak strength between -2.5 and

-1.25 eV, indicating that Fe and surface O atoms form bonding orbitals. Between 2.5 and 2.75 eV, Fe 3d orbital peak strength is greater than O 2p orbital peak strength, indicating that Fe and surface O atoms form weak anti-bonding orbitals. The observed layout value of Fe-O_s in Table 6 (0.32) can be attributed to the phenomenon where the electrons between Fe and the surface O occupy bonding states, resulting in the formation of a relatively stable chemical bond.

As demonstrated in Fig. 10(b), the contribution of Fe's 3d orbital electrons to the Fermi level reduces by half and the 3s orbital electrons vanish following the bidentate adsorption. The surface O atom's contribution to the 2p orbital electrons decreases substantially, and the non-localization of the s and p orbitals has been substantially enhanced. This implies the stability and activity of the Fe and surface O atoms after adsorption have both been significantly improved. Fig. 10b shows that following adsorption, Fe and O_u atoms produce new 3d orbital peaks and 2p orbital peaks in the ranges of 1.58–2.8 eV and -3.7–0.9 eV. After adsorption, the electrons of Fe and O_u atoms on the surface are filled with antibonding orbitals because the intensity of 3d orbital peaks is higher in the excited state than that of 2p orbital peaks. After adsorption, the Fe atom and surface O_u atom's electrons are filled with bonding orbitals because the 2p orbital peak in the ground state is stronger than the 3d orbital peak and has a broader range. In summary, the Fe-O_u bond layout value of 0.32, as presented in Table 6, corresponds to the prevailing bonding condition seen between the Fe atom and the surface O_u atom subsequent to adsorption. Similarly, the PDOS of O_t atoms appear more 2p impure peaks near the Fermi level, and produce new 2s orbital peaks in the range of -17.28 to -16.5 eV. These impure peaks correspond to the Fe 3d orbital peaks, which is also the reason why Fe and O_t atoms form bonding orbitals (corresponding layout value is 0.45).

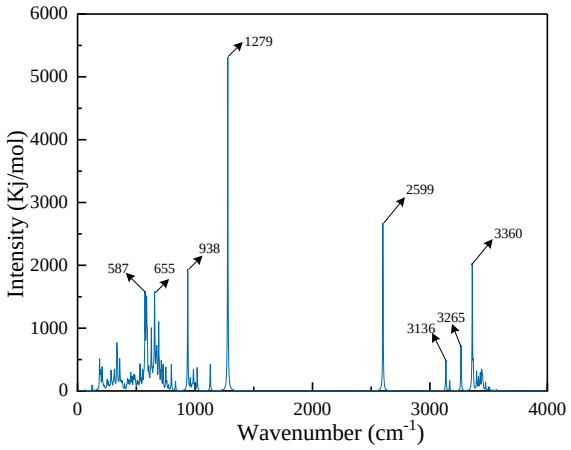

Fig. 11 Theoretical FT-IR calculations of UT-type compound

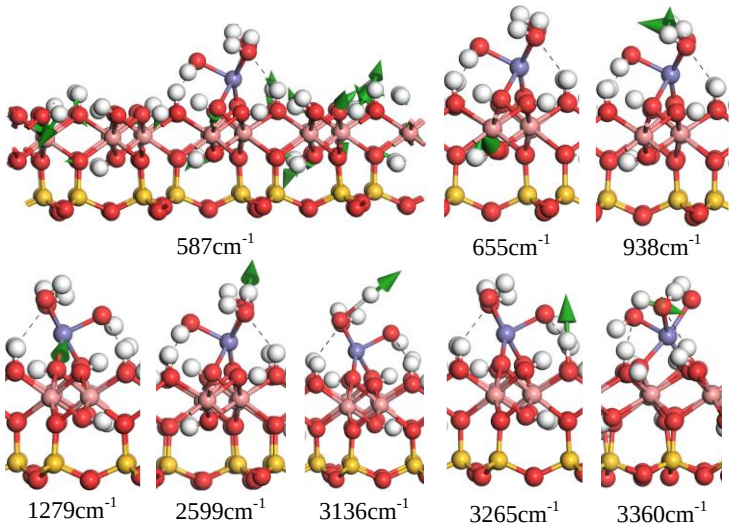

Fig. 12 Vibration images corresponding to different wavenumbers in Fig. 11

Fig. 11 presents the theoretical FT-IR calculations for the bidentate adsorption compound of hydrated $Fe(OH)_2^+$ on the surface of kaolinite. As depicted in the figure, multiple peaks with varying intensities appear at different wavenumbers. By analyzing the vibrations of these peaks with different intensities, the vibrational patterns of various chemical bonds within the adsorption compound are illustrated in Fig. 12. It is evident that the peak at 1279 cm^{-1} exhibits the highest intensity, and this peak arises from the stretching vibration of the Fe-O bond formed after the bidentate adsorption. This indicates that the adsorption of hydrated $Fe(OH)_2^+$ on the kaolinite surface is a result of chemical adsorption.

Furthermore, the peaks at 587 cm^{-1}, 655 cm^{-1}, 938 cm^{-1}, 2599 cm^{-1}, 3136 cm^{-1}, 3265 cm^{-1}, and 3360 cm^{-1} correspond to the vibrations of the hydroxyl groups on the kaolinite surface, vibrations of the inner Al-O bonds, bending vibrations of water molecules in the adsorbate, vibrations of hydroxyl groups in water molecules, vibrations of hydroxyl groups in the adsorbate, vibrations of hydrogen bonds, and stretching vibrations of hydroxyl groups in water molecules, respectively.

4. Conclusions

The study employed density functional theory (DFT) to investigate the primary constituent of hydrated $Fe(OH)_2^+$ in water environment. Additionally, the research examined the various adsorption configurations and mechanisms by which it occurs on the kaolinite (001) surface and the theoretical FT-IR calculations of bidentate adsorption compound was given to demonstrate the models are realistic. The findings of the investigation are presented as follows:

(1) When water is present, the predominant form of $Fe(OH)_2^+$ is $Fe(OH)_2(H_2O)_4^+$, which has a tendency to create an outer-sphere coordination adsorption compound through hydrogen bonding on the silica tetrahedral sheet of kaolinite. The production of a monodentate/bidentate compound on the alumina octahedral sheet of kaolinite is attributed to chemical bonding and hydrogen bonding. All three deprotonated oxygen atoms in the alumina octahedral sheet of kaolinite are linked to Fe atoms. After undergoing monodentate adsorption, the primary interaction of Fe atoms is with surface O_u atoms. However, in the case of bidentate adsorption, Fe atoms are prone to make surface connections with O_u and O_t atoms.

(2) Both types of compounds have strong bonding orbitals surrounding the Fe and surface O atoms, as evidenced by the bonding mechanism and Mulliken population analysis and theoretical FT-IR calculations show that the formation of Fe-O chemical bonds. The results of the study indicate a significant degree of covalency in the Fe-O_s bonds. The bidentate adsorption process, in comparison to monodentate adsorption, forms a greater number of chemical bonds, resulting in a bidentate adsorption compound that exhibits reduced energy, increased stability, and lower adsorption energy.

Acknowledgments

The authors gratefully acknowledge the support from the National Natural Science Foundation of China (No. 52274262 and 52004107), Jiangxi Province Key Disciplines Academic and Technical Leaders Training Program (20232BCJ23005), Jiangxi Province Outstanding Youth Fund (20232ACB214008), Jiangxi Natural Science Foundation (20224BAB204036), General Projects of Key R&D Programs of Jiangxi Province (20212BBG73049), National innovation and entrepreneurship Training Program for college students (202110407032).

References

CLARK, S.J., SEGALL, M.D., PICKARD, C.J., HASNIP, P.J., PROBERT, M.J., REFSON, K., PAYNE, M.C., 2005. *First principles methods using CASTEP*. Z Krist-Cryst Mater. 220, 567–570.

DOUSOVA, B., LHOTKA, M., GRYGAR, T., MACHOVIC, V., HERZOGOVA, L., 2011. *In situ co-adsorption of arsenic and iron/manganese ions on raw clays*. Applied Clay Science. 54(2), 166–171.

FANG, F., MIN, F., LIU, L., CHEN, J., REN, B., LIU, C., 2020. *Adsorption of $Al(OH)_n^{(3-n)+}$ (n =2–4) on kaolinite (001) surfaces: a DFT study*. Appl Clay Sci. 187, 105455.

FANG, X.H., XIA, Y.Y., QIU, T.S., ZHU, D.M., 2018. *Influence of tartaric acid on impurity leaching behavior of ionic rare earth ores*. Metal Mine. 6, 94–98.

FANG, X.H., ZHU, D.M., QIU, T.S., WU, H.Q., 2012. *Impurities inhibited leacning of the leach liquor of the weathered crust elution-deposited rare earth ore by adding aluminum inhibitor*. Nonferrous Metals Science and Engineering. 3, 51–55.

FENG, X., ONEL, O., COUNCIL-TROCHE, M., MACCORMAC, B.L., NOBLE, A., YOON, R.H., MORRIS, J.R., 2023. Rare earth ion-adsorption clays in the presence of iron at basic pH: Adsorption mechanism and extraction method. Applied Clay Science. 231, 106744.

HE, J.Y., LIU, R., WU, Y.X., ZHANG, Y., SUN, W., LI, G.S., CAO, Y.J., GAO, Z.Y., 2023. Surface hydration of zircon and its influence on the adsorption of typical flotation collectors: First-principle calculations. Applied Surface Science. 638, 158080.

HE, J.Y., ZHANG, H.L., YUE, T., SUN, W., HU, Y.H., ZHANG, C.Y., 2021. *Effects of hydration on the adsorption of benzohydroxamic acid on the lead-ion-activated cassiterite surface: a DFT study*. Langmuir. 37, 2205-2212.

IRETA, J., NEUGEBUERER, J., SCHEFFLER, M., 2004. *On the accuracy of DFT for describing hydrogen bonds: dependence on the bond directionality*. J. Phys. Chem. A. 108, 5692–5698.

JIANG, P.G., YU, X.B., XIAO, Y.Y., ZHAO, S., PENG, W.J., 2023. *Study on hydrogen adsorption on WO_3 (001) surface by density functional theory calculation*. Tungsten. 5(4), 558-569.

KOHN, W., SHAM, L.J., 1965. *Self-consistent equations including exchange and correlation effects*. Physical Review Journals. 140, A1133–A1138.

LIU, X.D., MEIJER, E.J., LU, X.C., WANG, R.C., 2012. *First-principles molecular dynamics insight into Fe^{2+} compounds adsorbed on edge surface of clay minerals*. Clays Clay Miner. 60, 341–347.

LUO, A.R., CHEN, J.H., 2022. *Effect of hydration and hydroxylation on the adsorption of metal ions on quartz surfaces: DFT study*. Appl. Surf. Sci. 595, 153553.

LUO, X.P., WEN, C.J., XU, J., MA, P.L., TANG, X.K., CHI, R.A., 2014. *Research prowess on and development trend of exploitation technique of ion-absorbed type rare earth ore*. Metal Mine. 6, 83–90.

MIAO, Y.Q., YAN, H.S., QIU, X.H., ZHOU, X.W., ZHU, D.M., LI, X.B., QIU, T.S., 2022. *Adsorption of hydrated Al^{3+} on the kaolinite (001) surface: A density functional theory study*. Appl Clay Sci. 225, 106498.

MONKHORST, H.J., PACK, J.D., 1976. *Special points for brillouin-zone integrations*. Phys. Rev. B. 13, 5188–5192.

MULLIKEN, R.S., 1955. *Electronic population analysis on LCAO–MO molecular wave functions*. J. Chem. Phys. 23, 1833–1840.

NEDER, R.B., BURGHAMMER, M., GRASL, T., SCHULZ, H., BRAM, A., FIEDLER, S., 1999. *Refinement of the kaolinite structure fromsingle-crystal synchrotron data*. Clays Clay Miner. 47, 487–494.

NEUMANN, A., OLSON, T. L., SCHERER, M. M., 2013. Spectroscopic Evidence for Fe(II)–Fe(III) Electron Transfer at Clay Mineral Edge and Basal Sites. Environmental Science & Technology, 47(13), 6969–6977.

PACK, J.D., MONKKORST, H.J., 1976. *Special points for brilliouin zone zategrations a reply*. Phys. Rev. B. 16, 1748–1749.

PENG, C., MIN, F., LIU, L., CHEN, J. 2017.*The adsorption of $CaOH^+$ on (001) basal and (010) edge surface of Na-montmorillonite: a DFT study: DFT study of adsorption of $CaOH^+$ on (001) Na-montmorillonite surface*. Surf Interface Anal. 49, 267–277.

PFROMMER, B.G., COTE, M., LOUIE, S.G., COHEN, M.L., 1997. *Relaxation of crystals with the quasi-Newton method*. J. Comput. Phys. 131, 233–240.

QIU, S., WU, H., YAN, H.S., LI, X.B., ZHOU, X.W., QIU, T.S., 2021. *Theoretical investigation of hydrated $[Lu(OH)_2]^+$ adsorption on kaolinite (001) surface with DFT calculations*. Appl. Surf. Sci. 565, 150473.

QIU, T.S., FANG, X.H., WU, H.Q., ZENG, Q.H., ZHU, D.M., 2014. *Leaching behaviors of iron and aluminum elements of ion-absorbed-rare-earth ore with a new impurity depressant*. Trans. Nonferrous Met. Soc. China. 24, 2986-2990.

QIU, T.S., QIU, S., WU, H., YAN, H.S., LI, X.B., ZHOU, X.W., 2021. *Adsorption of hydrated $[Y(OH)_2]^+$ on kaolinite (001) surface: Insight from DFT simulation*. Powder Technol. 387, 80-87.

QIU, T.S., ZHU, D.M., FANG, X.H., ZENG, Q.H., GAO, G.K., ZHU, H.L., 2014. *Leaching kinetics of ionic rare-earth in ammonia-nitrogen wastewater system added with impurity inhibitors*, Journal of Rare Earths. 32, 1175-1183.

VANDERBILT, D., 1990. *Soft self-consistent pseudopotentials in a generalized eigenvalue formalism*. Phys. Rev. B. 41, 7892–7895.

VITALY, A., KEVIN, M., 2013. *Insights into the Mechanism of Fe(II) Adsorption and Oxidation at Fe−Clay Mineral Surfaces from First-Principles Calculations*. J Phys Chem C. 117, 22880–22886.

WANG, J., XIA, S.W., YU, L.M., 2014. *Adsorption mechanism of hydrated $Pb(OH)^+$ on the kaolinite (001) surface*. Acta Physico-Chimica Sinica. 5, 829–835.

WANG, X.T., CHEN, Y.R., MI, J.Q., JIANG, J.W., JIANG, J., 2021. *Research status of leaching technology and leaching agent of ion-adsorption type rare earth ore*. World Nonferrous Metals. 22, 136–139.

WU, Z., COHEN, R.E., 2006. *More accurate generalized gradient approximation for solids*. Phys. Rev. B. 73, e235116.

WU, X.Y., ZHOU, F., XU, Y.L., FENG, J., CHI, R.A., 2021. *Research progress on the rare earth leaching agents of weathered crust elution-deposited rare earth ore*. Chinese Rare Earths. 42, 109–118.

XU, Y.H., 2005. *Removing of aluminum from praseodymium-neodymium carbonate*. Hydrometallurgy of China. 24, 92–94.

YAN, H.S., 2019. *First-principles study on the adsorption of hydrated rare earth ions on the surface of kaolinite*. Jiangxi: Jiangxi University of Science and Technology.

YIN, Z.G., HU, Y.H., SUN, W., ZHANG, C.Y., HE, J.Y., XU, Z.J., ZOU, J.X., 2018. *Adsorption mechanism of 4-Amino-5-mercapto-1,2,4-triazole as flotation reagent on chalcopyrite*. Langmuir. 34, 4071−4083.

YIN, J.Q., FU, G.M., WAN, Y., TIAN, J., 2012. *Development progress of extraction rare earths from the leach liquid of the weathered crust elution-deposited rare earth ore*. Jiangxi Science. 30, 574–578, 61.

ZHANG, H.L., SUN, W., ZHU, Y.G., HE, J.Y., CHEN, D.X., ZHANG, C.Y., 2021. *Effects of the goethite surface hydration microstructure on the adsorption of the collectors dodecylamine and sodium oleate*. Langmuir. 37, 10052-10060.

ZHANG, H.L., XU, Z.J., SUN, W., CHEN, D.X., LI, S., HAN, M.J., YU, H., ZHANG, C.Y., 2021. *Selective adsorption mechanism of dodecylamine on the hydrated surface of hematite and quartz*. Sep. Purif. Technol. 275, 119137.

ZHANG Z.J., ZHOU Q., YUAN Z.T., ZHAO L., DONG J.D., 2021. *Adsorption of Mg^{2+} and K^{+} on the kaolinite (001) surface in aqueous system: A combined DFT and AIMD study with an experimental verification*. Appl Sur Sci. 538, 148158.1-148158.8.

ZHANG, C., ZHANG, Q.J., HUANG, B., 2021. *Contamination prevention & control for ion-adsorbed rare earth deposit mining*. Energy Saving of Non-ferrous Metallurgy. 37, 46–49.

ZHAO, Z.H., SANG, X.Y., ZHANG, W.B., HAO, G.H., DUAN, C.K., LI, D., 2007. *Application of centrifuging sedimentation on removing aluminum and iron from rare earth solution*. Chinese Rare Earths. 28, 95–97.

ZHOU, F., HUANG, S.H., FENG, J., DENG, D.H., WANG, Z.W., LIU, Q., 2022. *Study on the distribution of rare earth ions and aluminum ions during the leaching of ammonium salts of weathered shell leaching rare earth minerals*. Chinese Journal of Nonferrous Metals. 32, 195–205.